Broadband Ground Motion Simulations for a Mw 7.8 Southern San Andreas Earthquake

2007 SCEC Annual Report

Robert Graves, Brad Aagaard and Ken Hudnut

Overview

Using the resources of the Community Modeling Environment of the Southern California Earthquake Center (SCEC), we compute broadband (0 – 10 Hz) ground motions over a large region of southern California for a M_w 7.8 rupture scenario of the southern San Andreas fault. The simulations incorporate a heterogeneous kinematic rupture description, as well as 3D complexity of the crust. Simulated near-fault PGA and PGV values generally range from 0.5 to 1.0 g and 100 to 250 cm/s, respectively. A southern hypocenter efficiently channels energy into the Los Angeles region along the string of basins lying south of the San Gabriel Mountains, while central and northern hypocenters are much less efficient at exciting this response. Comparison of the simulated motions with predictions from a recent NGA empirical ground motion model shows overall shaking levels that are generally within the expected scatter observed in prior events. The large density of broadband ground motions produced in these simulations facilitates the generation of high-resolution ground motion maps, which can be used as inputs for studies of damage potential and loss estimates.

Rupture Model Description

A detailed description of the spatial and temporal characteristics of the rupture has been developed for the ShakeOut exercise (Hudnut et al., 2007). The rupture extends 305 km along the Coachella and Mojave sections of the San Andreas fault from Bombay Beach, on the northeastern shore of the Salton Sea, to Lake Hughes, 20 km northwest of Palmdale. A slip predictable model describes the long lengthscale (wavelengths > 30 km) spatial distribution of slip. We incorporate shorter lengthscale variations (wavelengths between 0.5 km and 30 km) by adding random phase spatial variations that follow a wavenumber squared falloff (Somerville et al, 1999; Mai and Beroza, 2002). The background rupture speed is set to 85% of the local shear wavespeed, with local perturbations linearly correlated with slip. This is consistent with observations that ruptures tend to propagate faster in regions with larger slip as seen in spontaneous rupture models (e.g., Day, 1982) and inferred from source inversions of past earthquakes. The maximum rupture speed of 1.4 Vs corresponds to regions of maximum slip (16 m), regions of average slip (4 m) have a rupture speed of 0.85 Vs, and regions with negligible slip have a rupture speed of 0.2 Vs. Additionally, the rupture speed is tapered by 50% over 3 km along both the top and bottom edges of the rupture (consistent with rupture propagating from regions of unstable sliding to stable sliding). Slip initiation times are determined from this rupture speed distribution by tracing the rupture front away from the hypocenter assuming locally circular wave fronts. To complete the kinematic description, the slip time function is specified as a Brune pulse having a rise time that is proportional to the square root of slip. The rise time increases linearly over 5 km along the top and bottom edges of the rupture in a similar fashion to the decrease in rupture speed. This kinematic source model is mapped onto the detailed fault surface representation of the CFM, which includes variations in strike, dip, and fault width, resulting in a moment magnitude 7.8 earthquake.

Simulation Methodology

The broadband (0-10 Hz) ground motion simulations are computed using the hybrid procedure of Graves and Pitarka (2004), which has been validated using data from several earthquakes, including the 1989

Loma Prieta and 1994 Northridge events. This method combines a deterministic approach at long periods (T > 1 sec) with a semi-stochastic approach at short periods (T < 1 sec). The long period motions are calculated using a 3D visco-elastic, finite-difference algorithm with the 3D velocity structure derived from the SCEC CVM version 4.0 and the full kinematic rupture description. Anelastic attenuation is modeled using the relations $Q_s = 50\ V_s$ (V_s in km/s) and $Q_p = 2\ Q_s$. The long period computational domain covers a region 450 km by 225 km and extends to 45 km depth. We use a grid size of 0.125 km and a minimum shear velocity of 0.62 km/s. Over 2 billion grid nodes are required to represent this model and each calculation was performed using 520 CPUs at USC's center for High Performance Computing and Communication (HPCC). Each simulation required over 260 GB of RAM and took 24 hours to calculate 174 seconds (24,000 time steps) of simulated motion.

From the long period calculation, ground motions are saved on a 2 km resolution grid (25,500 sites) covering a large portion of southern California. For each of these sites, the short period motions are obtained using a methodology that sums the response for each subfault assuming a random phase and a wavenumber-squared source spectrum with an amplitude level scaled to the specified slip distribution. The approach follows from Boore (1983) with the extension to finite-faults given by Frankel (1995) and Hartzell et al. (1999). We include both direct and Moho-reflected rays, which are traced through a 1-D velocity model that roughly follows the average depth variations in the 3-D structure. For each ray we compute a radiation pattern coefficient by averaging over a range of slip mechanisms and take-off angles. Anelasticity is incorporated via a travel-time weighted average of the Q values for each of the material layers and a generic rock site spectral decay operator, k = 0.05. These simplified Green's functions are attenuated by 1/Rp, where Rp is the path length traveled by the particular ray with gross impedance effects included using quarter wavelength theory.

In order to account for site specific geologic conditions in the final broadband response, we apply period-dependent, non-linear amplification factors to the simulated time histories. These factors are based on the 30 m travel-time averaged shear wave speed (V_s^{30}) at the site of interest. The amplification factors are applied to the stochastic and deterministic responses separately since these have different reference site velocities. At each location in the simulation grid, we first obtain the site specific V_s^{30} (v_{site}) from the map of Wills et al. (2000) and then v_{ref} is set to either the Vs30 from the 3-D velocity model for that location (long period response) or the 1-D velocity model (short period response). Finally, we combine the individual stochastic and deterministic responses into a single broadband time history using a set of matched Butterworth filters (Hartzell et al., 1999).

Simulation Results

Broadband simulations for three rupture scenarios have been computed. The three scenarios all use the same slip distribution and only differ in hypocenter location; one located at the southern end of the fault (lon=-115.7068, lat=33.345, d=7.6 km), one located in the central portion of the fault along the San Gergonio Pass (lon=-116.7419, lat=34.0445, d=15.1 km), and one located at the northern end (lon=-118.2900, lat=34.6169, d=8.1 km)). For each of the 25,500 three-component ground motion time histories generated in the simulations, we process the motions to extract peak ground acceleration (PGA), peak ground velocity (PGV), and 5% damped spectral acceleration (SA) at a suite of oscillator periods. The high density of sites covered by the simulations facilitates the production of shaking maps for the various ground motion metrics. Figure 2 displays maps for PGA, SA at 1 second period and SA for 3 seconds period for the south hypocenter case. The SA values represent the geometric mean of the NS and EW horizontal components of motion.

The maps reveal many key features of the ground motion response for this scenario. At short periods (PGA), the motions are strongly influenced by proximity to the fault and slip distribution. The near fault PGA values generally range from 0.5 to 1 g, with the higher levels occurring along those fault sections

having the largest slip. Along the Coachella segment, a few sites very close to the fault have significantly larger PGA's with one site having a value of 2 g. These sites are immediately adjacent to the largest fault slip region of 16 m.

At longer periods (1 and 3 sec SA), the effects of rupture directivity and basin response become quite significant. For the southern hypocenter, the wave energy is strongly focused to the northwest along the direction of fault rupture. In addition, the coupling of rupture directivity towards the northwest with the channeling of energy into the string of basins lying south of the San Gabriel Mountains (San Bernardino, Chino, San Gabriel and Los Angeles) creates a very strong basin response in the Los Angeles region. This phenomenon has been documented for longer periods in the previous TeraShake simulations (Olsen et al., 2006). However, our results demonstrate that this effect appears at shorter periods as well, even affecting PGA values.

Figure 3 displays acceleration and velocity histories at three sites for the south hypocenter simulation. Station SVD is located about 1 km from the fault, PAS at 43 km and LBCH at 82 km. The motions at SVD are quite strong and relatively brief, primarily resulting from the effects of rupture directivity. The character and level of motions simulated at this site are similar to those recorded at similar distances during the 1992 Mw 7.3 Landers earthquake (Lucerne) and the 2002 Mw 7.9 Denali earthquake (Pump Station 10). At the more distant stations, the amplitude of the motions decreases and the duration of shaking increases. LBCH is located at the southern margin of the Los Angeles basin atop about 2.5 km of sediments. The large amplitude, later arriving energy at this site is comprised of basin generated surface waves that have propagated across the Los Angeles basin. The period of these waves is about 3 to 4 seconds.

Ruptures with the central and northern hypocenters also show very strong rupture directivity effects for the near fault region, although the spatial pattern of the strong shaking shifts with the hypocenter position. Whereas the south hypocenter concentrates the radiation of energy towards the northwest, the north hypocenter strongly focuses energy toward the southeast. The bilateral rupture of the central hypocenter directs strong shaking in both directions. As in the TeraShake simulations (Olsen et al., 2006) we find that the response of the Los Angeles basin is quite sensitive to the hypocenter location. The south hypocenter generates the strongest basin response, followed by the central, and then the north hypocenter, which excites a minimal response in the Los Angeles region.

References

Boore, D., 1983, Stochastic simulation of high frequency ground motions based on seismological models of the radiated spectra, *Bull. Seism. Soc. Am.*, **73**: 1865-1894.

Day, S., 1982, Three dimensional simulation of spontaneous rupture: The effect of non-uniform pre-stress, *Bull. Seism. Soc. Am.*, **72**, 1881-1902.

Frankel, A., 1995, Simulating strong motions of large earthquakes using recordings of small earthquakes: the Loma Prieta mainshock as a test case, *Bull. Seism. Soc. Am.*, **85**, 1144-1160.

Graves, R., and Pitarka, A., 2004, Broadband time history simulation using a hybrid approach, *Proc. 13th World Conf. Earthq. Eng.*, Vancouver, Canada, paper no. 1098.

Hartzell, S., Harmsen, S., Frankel, A., and Larsen, S., 1999, Calculation of broadband time histories of ground motion: comparison of methods and validation using strong ground motion from the 1994 Northridge earthquake, *Bull. Seism. Soc. Am.*, **89**, 1484-1504.

Hudnut, K., Jones, L., and Aagaard, B., 2007, The southern California ShakeOut scenario, part 1: Earth science specification of a big one, *Seism. Res. Lett.*, **78**, 264.

Mai, M., and Beroza, G., 2002, A spatial random field model to characterize complexity in earthquake slip, *J. Geophys., Res.*, **107**, B11.

Olsen, K., Day, S., Minster, J., Cui, Y., Chourasia, A., Faerman, M., Moore, R., Maechlin, P., and Jordan, T., 2006, Strong shaking in Los Angeles expected from a southern San Andreas earthquake, *Geophys. Res. Lett.*, **33**, L07305.

Somerville, P., Irikura, K., Graves, R., Sawada, S., Wald, D., Abrahamson, N., Iwasaki, Y., Kagawa, T., Smith, N., and Kowada, A., 1999, Characterizing crustal earthquake slip models for the prediction of strong ground motion, *Seism. Res. Lett.*, **70**, 199–222.

Wills C., Petersen, M., Bryant, W., Reichle, M., Saucedo, G., Tan, S., Taylor, G., and Treiman, J., 2000, A site conditions map for California based on geology and shear wave velocity, *Bull. Seism. Soc. Am.*, **90**(6B), S187-S208.

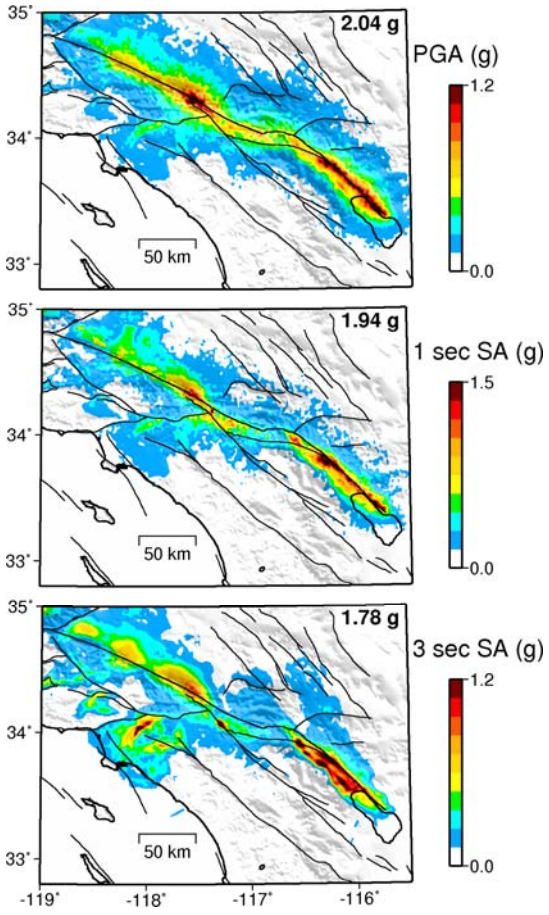

Figure 1. Maps of simulated PGA (top), SA at 1 sec (middle), and SA at 3 sec (bottom) for the south hypocenter case. The maximum value for each map is indicated in the upper right corner of each panel (color scale is clipped for display clarity)

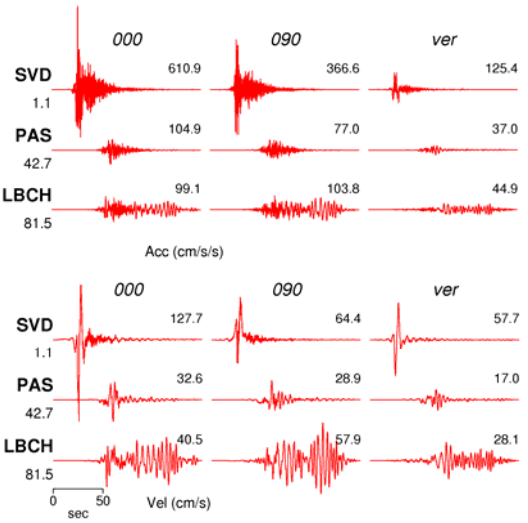

Figure 2. Three component acceleration (top set) and velocity (bottom set) time histories simulated at Seven Oaks Dam (SVD), Pasadena (PAS) and Long Beach (LBCH). The distance (in km) to the fault for each site is listed below the station code. Each set of traces is plotted on the same scale.

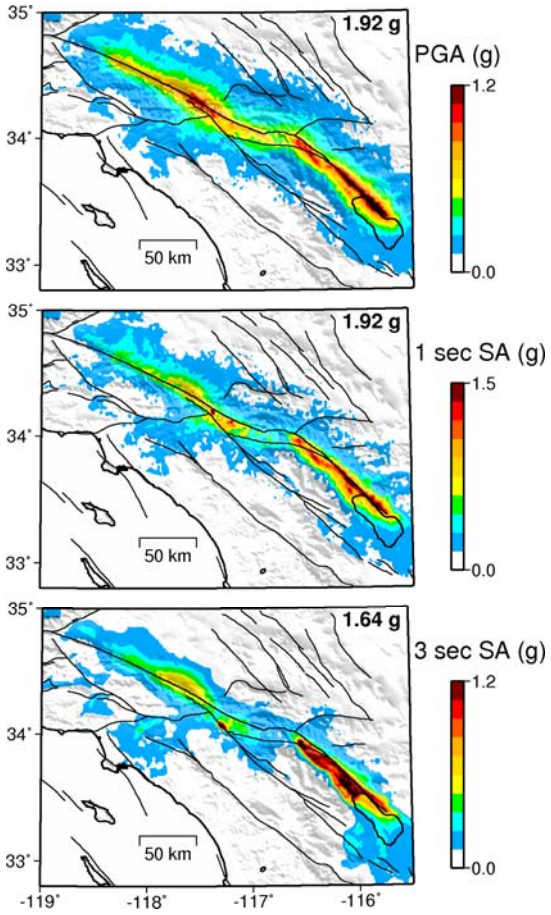

Figure 3. Maps of simulated PGA (top), SA at 1 sec (middle) and SA at 3 sec (bottom) averaged over the three hypocenters. The maximum value for each map is indicated in the upper right corner of each panel (color scale is clipped for display clarity).

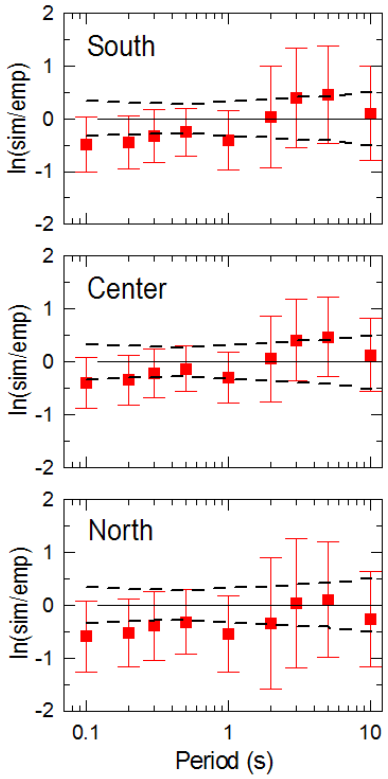

Figure 4. Red squares plot average of residuals between simulations and empirical predictions from model CB08 as a function of period for the three hypocenter cases. Positive values indicate the simulations predict larger motions than the empirical model; negative values indicate smaller simulated values compared to the empirical model. The error bars indicate +/- 1 standard error for the residuals. The heavy dashed line plots the +/- 1 standard error level of the inter-event term from the empirical model.